coatings

MDPI

Article

Development of Silver Doped Hydroxyapatite Thin Films for Biomedical Applications

Simona Liliana Iconaru [1], Daniela Predoi [1,*], Carmen Steluta Ciobanu [1], Mikael Motelica-Heino [2], Régis Guegan [3] and Coralia Bleotu [4,5,*]

1 National Institute of Materials Physics, Atomistilor Street, No. 405A, P.O. Box MG 07, 077125 Magurele, Romania; simonaiconaru@gmail.com (S.L.I.); ciobanucs@gmail.com (C.S.C.)
2 Department of Civil Engineering and Environment, Université d'Orléans, ISTO, UMR 7327 CNRS, 1A Rue de la Férollerie, 45071 Orléans, France; mikael.motelica@univ-orleans.fr
3 Global Center for Science and Engineering, Waseda University, Tokyo 169-8555, Japan; regis.guegan@aoni.waseda.jp
4 Stefan Nicolau Virology Institute, 030304 Bucharest, Romania
5 Life, Environmental and Earth Sciences Division, Research Institute of the University of Bucharest (ICUB), University of Bucharest, 060023 Bucharest, Romania
* Correspondence: dpredoi@gmail.com (D.P.); coralia.bleotu@virology.ro (C.B.)

Abstract: Silver doped hydroxyapatite [AgHAp, $Ca_{10-x}Ag(PO_4)_6(OH)_2$], due to its antimicrobial properties, is an advantageous material to be used for various coatings. The AgHAp thin films with x_{Ag} = 0.05 and x_{Ag} = 0.1 were achieved using the spin-coating method. The resulting samples were examined by X-ray diffraction (XRD), scanning electron microscopy (SEM), atomic force microscopy (AFM), Fourier transform infrared spectroscopy (FTIR), Raman spectroscopy, and X-ray photoelectron spectroscopy (XPS). XRD analysis revealed that the particles of both samples are ellipsoidal. Also, in agreement with the results obtained by XRD measurements, the results of the SEM studies have shown that the particles shape is ellipsoidal. Optical properties of silver doped hydroxyapatite thin films deposited on Si substrate were investigated through Fourier transform infrared spectroscopy (FTIR) and Raman spectroscopy. The results obtained by the two complementary techniques highlighted that the molecular structure of the studied samples is not influenced by the increase of the silver concentration in the samples. Our studies revealed that the surface morphology of the obtained samples consist of uniform and continuous layers. The biocompatibility of the obtained thin films was also evaluated with the aid of human osteosarcoma MG63 (ATCC CRL 1427) cell line. Moreover, the in vitro antifungal activity against *Candida albicans* fungal strain of the AgHAp thin films was studied and the obtained results revealed their antifungal effect. The results of the biological assays showed that the AgHAp thin films are a very promising material for biomedical applications.

Keywords: silver; hydroxyapatite; thin films; biocompatibility; surface morphology

Citation: Iconaru, S.L.; Predoi, D.; Ciobanu, C.S.; Motelica-Heino, M.; Guegan, R.; Bleotu, C. Development of Silver Doped Hydroxyapatite Thin Films for Biomedical Applications. *Coatings* **2022**, *12*, 341. https://doi.org/10.3390/coatings12030341

Academic Editor: Maria Cristina Tanzi

Received: 15 January 2022
Accepted: 3 March 2022
Published: 5 March 2022

1. Introduction

Hydroxyapatite (HAp) is one of the most extensively studied materials for biomedical applications due to its extraordinarily properties such as biocompatibility, bioactivity, and osteoconductivity. The HAp properties are derived mostly from the structural and chemical similarities that this material shares with the mineral component of the mammalian bone [1–3]. Synthetic hydroxyapatite is one of the most common materials used for implantable devices as a coating on metallic prostheses to improve the biological response of the host's surrounding tissue [4–6]. Previous studies have revealed that the use of HAp as coating could facilitate the fixation of the implant, as well as the bonding between the host bone and the implant, and that it could also improve and sometimes even accelerate bone growth from the bone/implant interface [4–8]. During recent years, due to a rapid

emergence of drug-resistant microorganisms and to an increase of implant-associated infections, recent advances in the field of novel antimicrobial materials with high biocompatible properties have been in demand from the medical community [4–9]. In general, when a post-implant infection occurs, it is due to the formation of microbial biofilms (which occur as a result of the rapid development and proliferation of infectious agents) [4–10]. Usually, these microbial biofilms are very difficult to treat with conventional antibiotics. In these cases, implant removal and replacement is the only method to eliminate severe infections, which could even lead to patient's death. This could exert both physical and financial stress on the patients, and therefore materials with both antibacterial and biocompatible properties are highly desired [10–16]. Studies have shown that silver (Ag) has been one of the best agents to control bacterial adhesion and prevent biofilm formation. Silver has been known since ancient times for its broad antibacterial spectrum and oligodynamic bactericidal activity in different biomedical fields, and has been intensively studied due to its antimicrobial properties [10–18]. Also, silver is effective against a wide range of drug-resistant microorganisms and has been approved for use in various medical devices for over 20 years [19–21]. Recent studies have emphasized that using a doped HAp coating could help improve its osteoconductivity (depending on the dopant ion) and could confer other improvements to the conventional HAp coating such as antimicrobial and osteogenic properties [17–22]. Previous studies reported obtaining silver-doped hydroxyapatite and have demonstrated its antimicrobial properties [16–22]. Besides, a high concentration of Ag can be toxic and lead to severe disease if not properly quantified in the hydroxyapatite structure (and if there is no Ag^+ ions controlled release) [23,24]. High concentrations of silver are responsible for affections such as leukopenia and liver and kidney damage. Also, long-time exposure to silver in human blood that exceeds the threshold limit can cause argyria in the human body [25]. In this context, the optimization of silver concentration in the HAp lattice is of critical importance to be able to guarantee the obtaining of Ag/HAp optimal antimicrobial activity of the samples without exhibiting any cytotoxicity. Therefore, studies regarding the development of silver doped antimicrobial coatings for biomedical applications that could be used to reduce the apparition of implant-related post-operatory infections and that also exhibits biocompatible properties are of great concern to the scientific community worldwide. In their studies, Qing et al. [26,27] reported that silver nanoparticles could influence bone origin and affect the development of morphological characteristics in various injuries, demonstrating an osteogenic potential towards human urine derived stem cells. In addition, the studies reported by Mahmood et al. [28] demonstrated that silver nanoparticles have the potential to significantly enhance the osteoblast lineage in MC3T3-E1 cell differentiation and mineralization in vitro.

In this context, this study aimed to evidence that silver doped hydroxyapatite thin films [AgHAp, $Ca_{10-x}Ag(PO_4)_6(OH)_2$] with x_{Ag} = 0.05 (0.05 AgHAp) and x_{Ag} = 0.1 (0.1 AgHAp) obtained by spin-coating technique are a promising material to be used in various medical applications. Both AgHAp samples were analyzed by various techniques such as X-ray diffraction (XRD), scanning electron microscopy (SEM), atomic force microscopy (AFM), Fourier transforms infrared spectroscopy (FTIR), Raman spectroscopy, and X-ray photoelectron spectroscopy (XPS). Moreover, the biocompatibility of the obtained thin films was evaluated using human osteosarcoma MG63 (ATCC CRL1427) cell line. in vitro antifungal activity of the thin films was also evaluated using *Candida albicans* ATCC 10231 fungal strain. This study's novelty mainly consists in the development of AgHAp thin films on Si substrate and their complex characterization from both a physico-chemical and biological point of view. Also, the results of morphological studies conducted on the thin films were reported for the first time. Furthermore, we report for the first time information regarding the attachment and proliferation of MG63 cells on HAp and AgHAp thin film's surface by AFM studies.

2. Materials and Methods

2.1. Materials

All of the necessary reagents for the synthesis including ammonium dihydrogen phosphate [$(NH_4)_2HPO_4$], calcium nitrate [$Ca(NO_3)_2 \cdot 4H_2O$], and silver nitrate $AgNO_3$ were purchased from Alpha Aesare (Kandel, Germany). All of the reagents were used without prior purification [29].

2.2. Silver Doped Hydroxyapatite Thin Films Using Spin-Coating Technique

The silver doped hydroxyapatite [AgHAp, $Ca_{10-x}Ag_x(PO4)_6(OH)_2$] suspension, with x_{Ag} = 0; 0.05 and 0.1, was prepared by coprecipitation using $AgNO_3$, $(NH_4)_2HPO_4$ and $Ca(NO_3)_2 \cdot 4H_2O$ in agreement with previous research [29]. The [Ca+Ag]/P molar ratio was 1.67. The final volume of [Ca+Ag]-containing solution ($AgNO_3$ and $Ca(NO_3)_2 \cdot 4H_2O$ dissolved in water) was 300 mL. The final volume of P-containing solution ($(NH_4)_2HPO_4$ was dissolved in deionized water) was 300mL, too. The solution containing Ca and Ag was stirred at 100 °C for 30 min. After that, the P-containing solution was added into the [Ca+Ag]-containing solution and stirred for 2 h. The pH value was adjusted at 10 by adding NH_3. The final solution was centrifuged and redispersed in deionized water for five times. The final suspension was aged at 40 °C for 12 h. The coatings on Si substrate were realized by spin-coated method. For this purpose, 0.3 mL of AgHAp (x_{Ag} = 0; 0.05 and 0.1) suspension was deposited on Si substrate at 3500 rpm. The time of deposition was equal to 10 s. The procedure of obtaining the AgHAp coatings was repeated three times. Each layer was treated in air at room temperature, for 2 h. After the final treatment at room temperature, the coatings were calcined in an oven at 600 °C for 2 h (heating rate 2 °C/min) in order to acquire the final AgHAp films.

2.3. Characterization Methods

The crystalline structure of the AgHAp thin films was examined by X-ray diffraction (XRD). The AgHAp thin film was measured in grazing incidence (GIXRD) geometry, with a Rigaku SmartLab 3 kW equipment (Rigaku, Tokyo, Japan), using CuK_α radiation (λ = 1.5418 Å) and an incidence angle of 0.5° [30]. The patterns were acquired in the 2θ range 15–70°, with a step size of 0.02°, and a dwell time of 8.5 s.

SCIENCE SES 2002 system and a monochromatic source of the X-ray radiation Al K_α (hν = 1486.6 eV) were used to collect X-ray photoelectron spectroscopy (XPS, Scienta Omicron, Taunusstein, Germany) data. All samples were recorded to have the carbon (C 1 s) peak for sp2 carbon at a binding energy of 284.8 eV. All XPS data were processed using the Casa XPS 2.3.14 software (version: 2.3.14) [31].

The surface morphology of the obtained coatings was analyzed by scanning electron microscopy with the aid of a Hitachi S4500 equipment (Hitachi, Tokyo, Japan). The 3D reconstruction of the 2D SEM micrographs was carried out with Image J software (ImageJ 1.51j8, National Institutes of Health, Bethesda, MD, USA) [32].

Additional data regarding the morphology of the coatings was obtained using an inversed trinocular metallographic microscope OX.2153-PLM (Euromex, Arnhem, The Netherlands). The images were recorded using the 10X magnification and the 2D metallographic images obtained were represented in 3D with the aid of Image J software (ImageJ 1.51j8, National Institutes of Health, Bethesda, MD, USA) [32].

Information about the surface topography of the coatings was also obtained using atomic force microscopy (AFM, NT-MDT, Moscow, Russia) technique. For this purpose, a NT-MDT NTEGRA Probe Nano Laboratory instrument (NT-MDT, Moscow, Russia) was used. The instrument was operated in non-contact mode using a silicon NT-MDT NSG01 cantilever (NT-MDT, Moscow, Russia) coated with a 35 nm gold layer. The data was recorded at room temperature. The AFM topography was acquired on a surface area of 3 μm × 3 μm. The AFM recorded data was processed with the aid of Gwyddion 2.59 software (Department of Nanometrology, Czech Metrology Institute, Brno, Czech Republic) [33].

Fourier-transform infrared spectroscopy (FTIR) measurements were achieved using a SP 100 Perkin Elmer spectrophotometer (PerkinElmer, Waltham, MS, USA) operated in Attenuated total reflectance mode (ATR-FTIR, PerkinElmer, Waltham, MS, USA). The spectra were acquired in the 4000–400 cm^{-1} spectral range with a resolution of 4 cm^{-1}.

In order to obtain the Raman spectra, a Renishaw InVia dispersive Raman spectrometer (excitation line of 514 nm provided by (gas-type) Spectra Physics Argon laser (20 mW) and 1800 L/mm gratings) was used. The spectrometer was equipped with a Leica DM microscope (Renishaw, Wotton-under-Edge, UK). The Raman spectra were collected in the 0–1200 cm^{-1} spectral range with a resolution of 2 cm^{-1}.

2.4. Biological Evaluation

Growth of human osteosarcoma MG63 (ATCC CRL1427) cells was carried out using Dulbecco's Modified Eagle's Medium: F12 (DMEM:F12, Sigma–Aldrich, St. Louis, MO, USA) supplemented with 10% Gibco Fetal Bovine Serum (FBS, Life Technologies Ltd., Renfrew, UK). The cells were maintained at 37 °C in a humidified atmosphere and 5% CO_2. The cells were grown in flasks with filter screw caps (TPP, Trasadingen, Switzerland) until the monolayer confluence and sub-cultivated in complete medium in a 1:3 split ratio.

Each HAp and AgHAp thin films, which covered a 0.5 mm square of Si, was placed in 24-well plates and exposed to UV light for one hour on each side for sterilization. MG63 (ATCC CRL1427) cells were added at a 1×10^5/well concentration in a complete medium and maintained at 37 °C for 48 h. The morphology of the cells next to the square of the material was checked under a visible light using an Axio Observer Inverted microscope (Carl Zeiss, GMBH, Munich, Germany). In order to observe the morphology of the cells grown on thin films, the cells were fixed in 70% ethanol and then stained with 50 mg/mL propidium iodide in the dark or with a combination of 1mg/mL acridine orange and 1mg/mL mitotraker red and observed at Zeiss Axio Observer microscope equipped with fluorescence module. Additional information regarding the attachment and proliferation of the cells on the HAp and AgHAp thin film's surface was obtained by AFM studies. For this purpose, the cells were fixed in 70% ethanol and then AFM topographies of the thin films were acquired on a surface area of 40 μm × 40 μm at room temperature using the NT-MDT NTEGRA Probe Nano Laboratory instrument previously described.

For cell cycle analysis, the cells were detached with trypsin, washed in PBS, fixed in 70% cold ethanol, and then kept overnight to −20 °C. The cells were rehydrated with PBS, treated with RNase A (1 mg/mL) and stained with propidium iodide (100 mg/mL) at 37 °C for 1 h. The changes in cellular DNA content were measured using EPICS XL flow cytometer (Beckman Coulter, Brea, CA, USA) and analyzed with FlowJo 8.8.6 software program (Ashland, OR, USA).

In vitro antifungal activity of the thin films was also evaluated using *Candida albicans* ATCC 10231 fungal strain. The in vitro antifungal assays were performed as previously described in [34] and the antifungal activity of the thin films was assessed after 48 h of incubation with the fungal suspensions. The qualitative antifungal evaluation was carried out with the aid of scanning electron microscopy (SEM) and confocal laser scanning microscopy (CLSM, Leica, Wetzlar, Germany). The detail of the experimental procedure was also detailed in [34]. The experiments were carried out in triplicate and the results were presented as mean ± SD.

3. Results

The X-ray diffraction method was used to establish the average particle size of HAp and AgHAp thin films (x_{Ag} = 0, x_{Ag} = 0.05 and x_{Ag} = 0.1). Figure 1 shows the XRD patterns of the HAp, 0.05 AgHAp and 0.1 AgHAp thin films. In this study, the Joint Committee on Powder Diffraction Standards (JCPDS) file for pure HAp (PDF No. 09-0432) was used as reference. The Debye–Scherrer formula [35–38] allowed the calculation of the average particle size. The diffraction peaks corresponding to planes (300) and (002) of AgHAp thin films (x_{Ag} = 0, x_{Ag} = 0.05 and x_{Ag} = 0.1) were used to determine the particle size and lattice

constants (Table 1). As shown in Table 1, the particle size increased along with the a-axis of its crystal plane, which shows that the particles have an ellipsoidal shape for both samples studied.

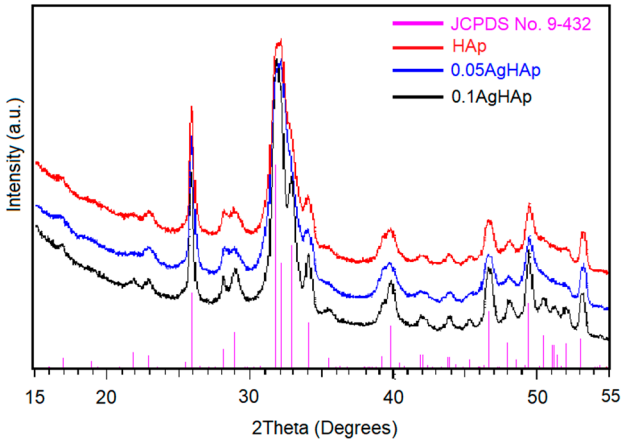

Figure 1. XRD patterns of the HAp in red, 0.05 AgHAp in blue, 0.1 AgHAp in black and of pure hydroxyapatite (JCPDS no. 9-0432) in pink.

Table 1. Lattice constant and crystalline sizes calculated from the XRD patterns of the HAp, 0.05 AgHAp and 0.1 AgHAp thin films.

Sample	Lattice Constant		Crystalline Size	
	a (Å)	c (Å)	d_{300} (Å)	d_{002} (Å)
HAp (JCPDS card No. 09-432)	9.416	6.874	-	-
HAp	9.418	6. 878	17.98	24.87
0.05 AgHAp	9.421	6.883	16.34	22.91
0.1 AgHAp	9.421	6.883	15.15	21.31

The qualitative evaluation of the surface components and composition of the 0.05 AgHAp thin film, was performed using the XPS technique. The survey XPS narrow scan spectra of the 0.05 AgHAp thin film is presented in Figure 2A. Figure 2B depicts the spectra of Ag element for the 0.05 AgHAp thin film. In the XPS general spectrum of 0.05 AgHAp thin film the peaks corresponding to the binding energy (BE) of the constituent elements: Ca (2p, 347.3 eV), O (1s, 532.1 eV), P (2p, 133.09 eV), and Ag (3d, 368.09 eV) were observed. The peak of Ag ($Ag(3d_{3/2})$ was identified at BE of 368.4 eV and peak of $Ag(3d_{5/2})$ was observed at BE of 374.3 eV in good agreement with previous studies [39,40]. The high resolution XPS spectra of Ag element was presented in Figure 2B.

The surface morphology of HAp, 0.05 AgHAp and 0.1 AgHAp coatings was investigated using three different techniques scanning electron microscopy, metallographic microscopy, and atomic force microscopy. The images obtained by SEM studies are depicted in Figure 3a–f. The results obtained by SEM revealed that all of the investigated coatings presented a homogenous and uniform surface without any noticeable cracks or unevenness. Moreover, the SEM data also highlighted that the particles have nanometric dimensions and an ellipsoidal shape. In addition, the SEM micrographs also suggested that the coatings present a uniform morphology and are composed of nanometric particles conglomerates. Those findings are in agreement with the XRD results. Furthermore, the 3D representation of the SEM micrographs also emphasized that the coatings have the aspect of uniform layers with no visible fissures, cracks, or other impurities.

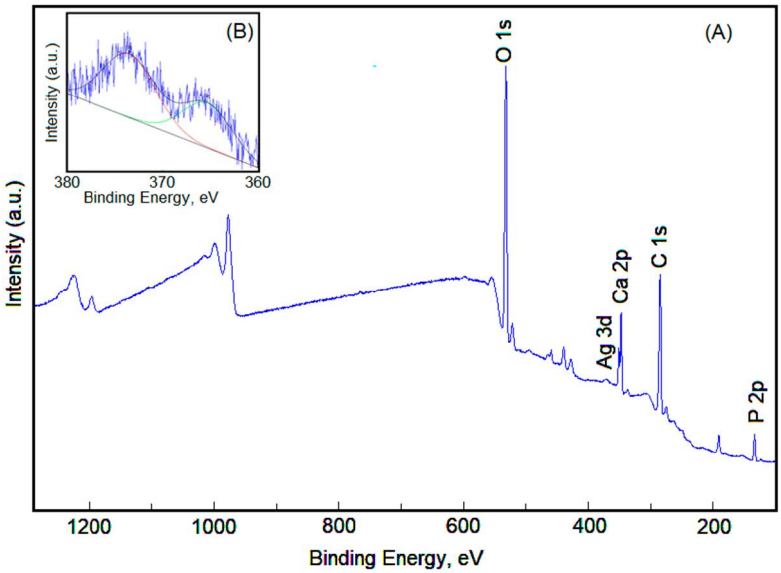

Figure 2. XPS general spectrum of 0.05 AgHAp thin film (**A**). The high resolution XPS spectra of Ag (3d) XPS peak of 0.05 AgHAp thin film (**B**).

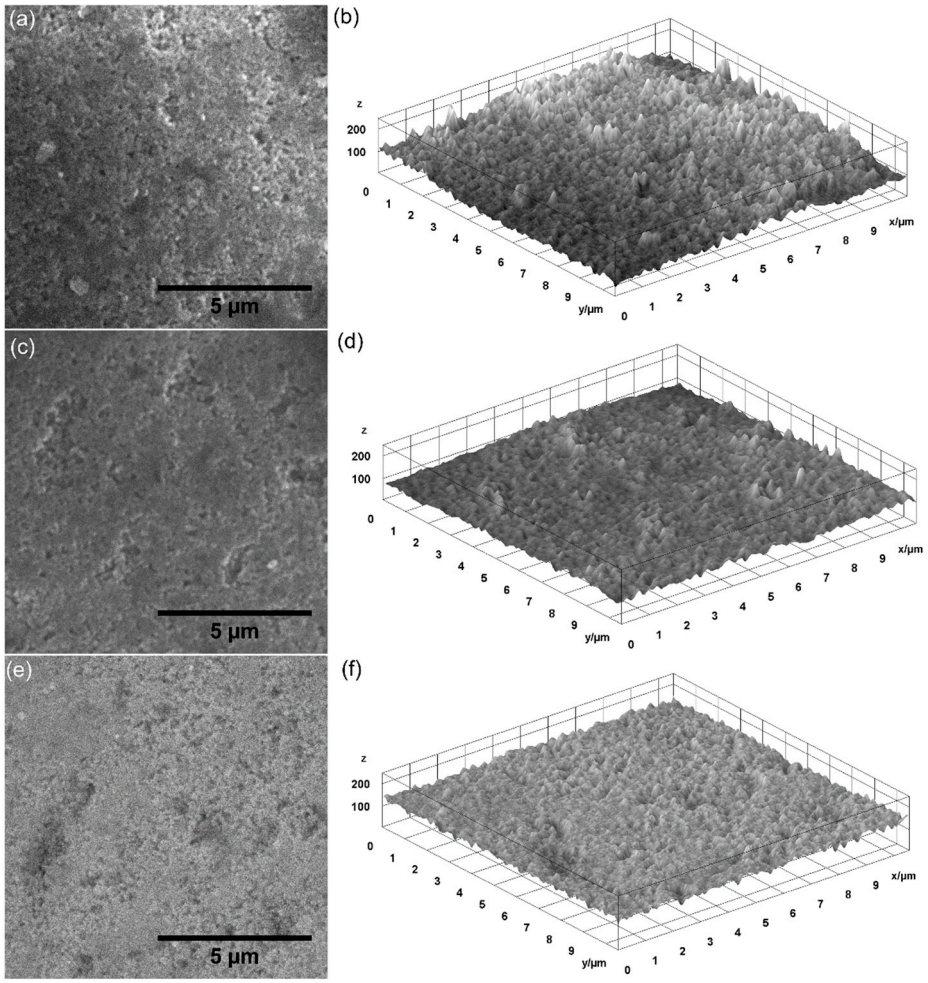

Figure 3. 2D SEM micrographs of HAp (**a**), 0.05 AgHAp (**c**), 0.1 AgHAp (**e**) coatings and 3D representation of SEM micrographs of HAp (**b**), 0.05 AgHAp (**d**), and 0.1 AgHAp (**f**) coatings.

Studies regarding the surface morphology of the HAp, 0.05 AgHAp, and 0.1 AgHAp coatings were also perfomed using metallographic microscopy. The 2D metallographic microscopy images of HAp, 0.05 AgHAp and 0.1 AgHAp coatings and their 3D reconstruction are presented in Figure 4a–f. In good agreement with the SEM studies, the metallographic microscopy images highlighted that the obtained coatings were uniformly deposited and did not present any cracks or fissures or any other impurities on their surface. More than that, the images showed that the coatings are comprised of nanometric particle conglomerates.

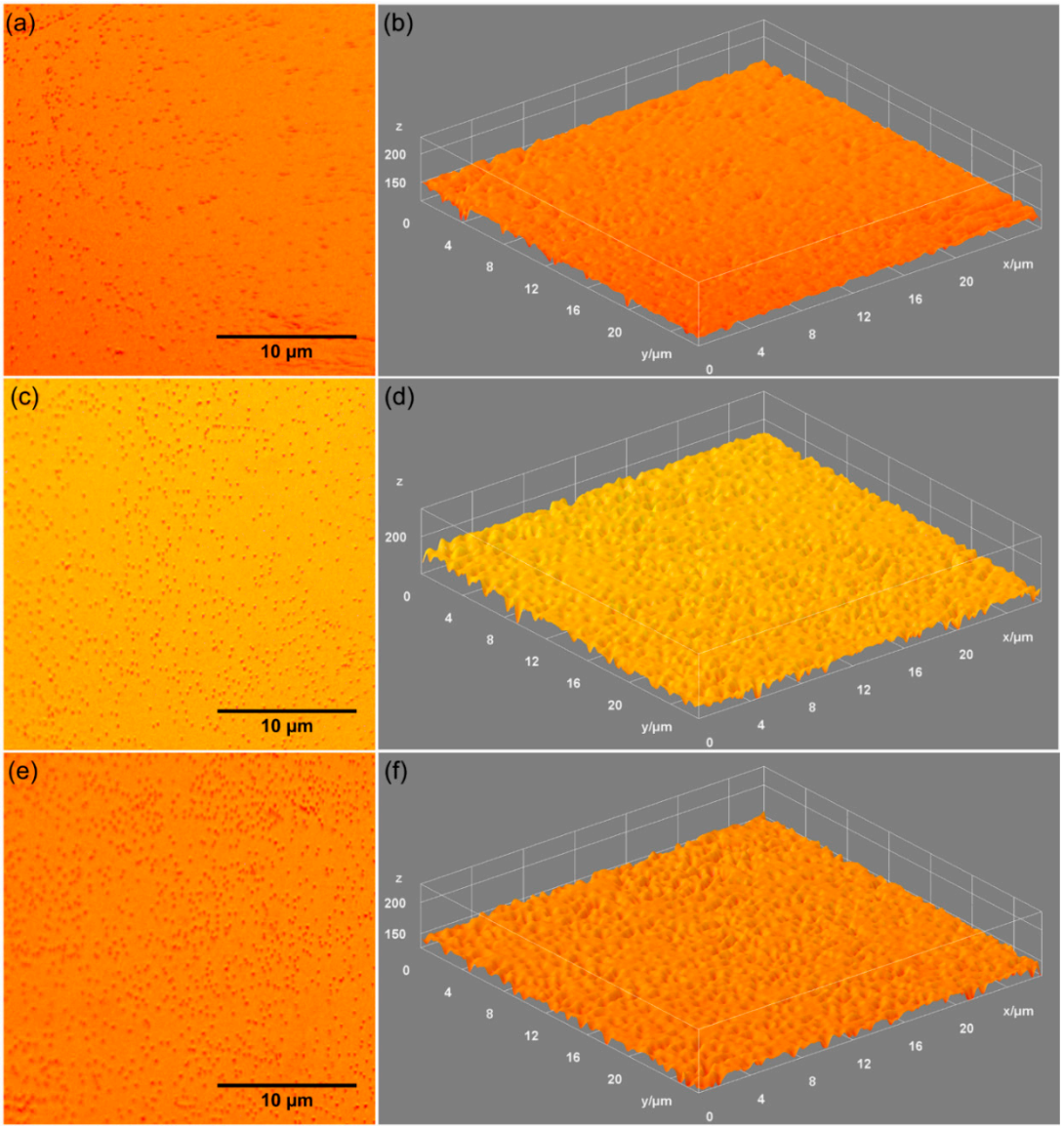

Figure 4. 2D Metallographic images (taken using 10× magnification) of HAp (**a**), 0.05 AgHAp (**c**), and 0.1 AgHAp (**e**) coatings, and 3D representation of the metallographic images of HAp (**b**), 0.05 AgHAp (**d**), and 0.1 AgHAp (**f**) coatings.

Complementary studies regarding the morphology of the HAp, 0.05 AgHAp and 0.1 AgHAp coating's surface was performed using AFM technique. AFM 2D topographies of the HAp, 0.05 AgHAp, and 0.1 AgHAp coating's surface as well as their 3D representation are depicted in Figure 5a–f. The AFM topographies recorded on a surface of 3 µm × 3 µm suggested that the coatings are continuous and uniform. Moreover, both 2D AFM topographies and their 3D representation emphasized that the coatings have the aspect of a homogenous and uniformly deposited layer with no visible fissures, cracks, or other

impurities on their surface. In addition, the roughness parameters of the HAp, 0.05 AgHAp and 0.1 AgHAp coatings were also calculated. The root mean square roughness (R_{RMS}) values obtained for the analyzed samples are presented in Table 2. The results obtained for the R_{RMS} roughness parameter confirmed the visual investigations and highlighted that the surface of HAp, 0.05 AgHAp, and 0.1 AgHAp coatings presented a homogenous and uniform morphology (with a diminished roughness). Moreover, the results obtained by AFM studies are in good agreement with the results obtained by other complementary methods, such as SEM and metallographic microscopy.

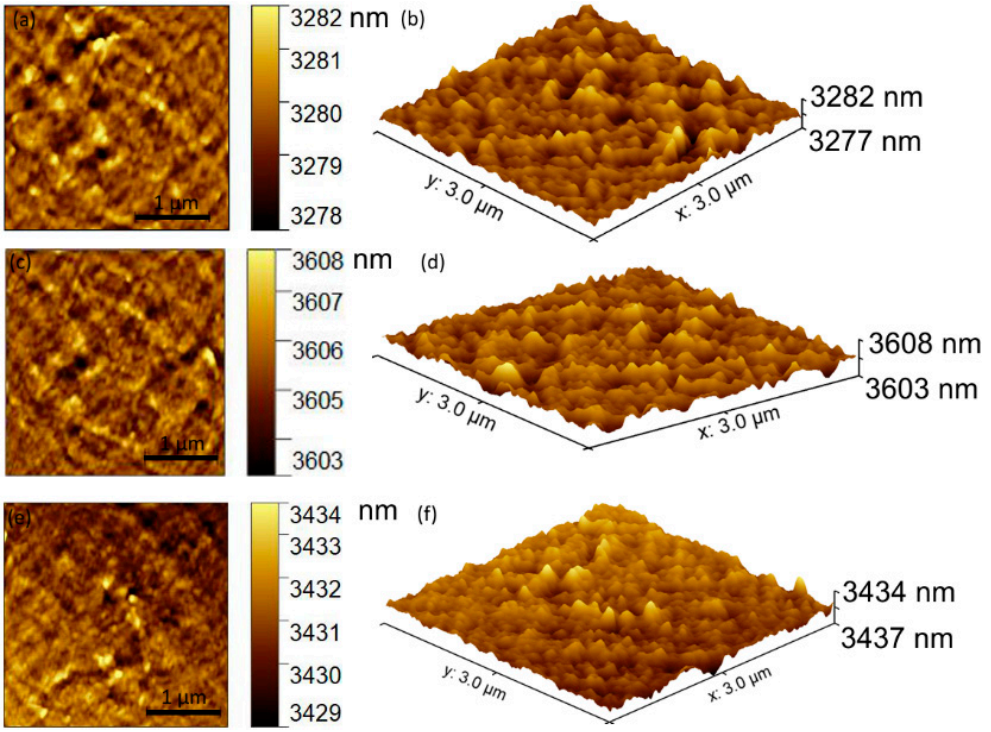

Figure 5. 2D AFM topography of HAp (**a**), 0.05 AgHAp (**c**), and 0.1 AgHAp (**e**) coatings and 3D representation of the 2D AFM topographies of HAp (**b**), 0.05 AgHAp (**d**), and 0.1 AgHAp (**f**) coatings.

Table 2. Root mean square roughness (R_{RMS}) value for HAp, 0.05 AgHAp, and 0.1 AgHAp coatings.

Sample	R_{RMS}
HAp	7.92 nm
0.05 AgHAp	6.26 nm
0.1 AgHAp	6.20 nm

Optical properties of silver doped hydroxyapatite (x_{Ag} = 0; 0.05 and 0.1) thin films deposited on Si substrate were studied with the aid of two complementary techniques, namely Fourier transform infrared spectroscopy (FTIR) and Raman spectroscopy. The results of the Fourier transform infrared spectroscopy (FTIR) studies are presented in Figure 6. In the following, we will discuss the FTIR spectra obtained on pure hydroxyapatite films, since the other two FTIR spectra (obtained for x_{Ag} = 0.05 and 0.1 thin films) are similar to this one. Therefore, as shown in Figure 6, our studies highlighted the presence of the main functional groups characteristic to the hydroxyapatite structure (phosphate and hydroxyl groups, respectively) in all of the analyzed samples. The vibrational bands, which are characteristic to the phosphate groups (PO_4^{3-}) from the hydroxyapatite structure could be noticed at about 474 cm^{-1} (ν_2), 564 cm^{-1} (ν_4), 604 cm^{-1} (ν_4), 961 cm^{-1} (ν_1), and 1032–1094 cm^{-1} (ν_3) [41–43]. The FTIR maxima present at around 635 cm^{-1} belongs to the structural OH groups (stretching and vibrational modes). Moreover, the broad bands that are observed in 3200–3600 cm^{-1} spectral region are specific to the H–O–H bands of

water lattice, while the vibrational band from 1632 cm^{-1} is characteristic to the adsorbed water [41–43]. The FTIR maxima observed at about 1453 and 1407 cm^{-1} could be attributed to CO_3^{2-} groups presented in the analyzed thin films. Also, the peak at around 874 cm^{-1} is characteristic to HPO_4^{2-} [41]. In the obtained FTIR spectra, it can be seen that after silver doping of pure hydroxyapatite, its structure does not undergo significant changes.

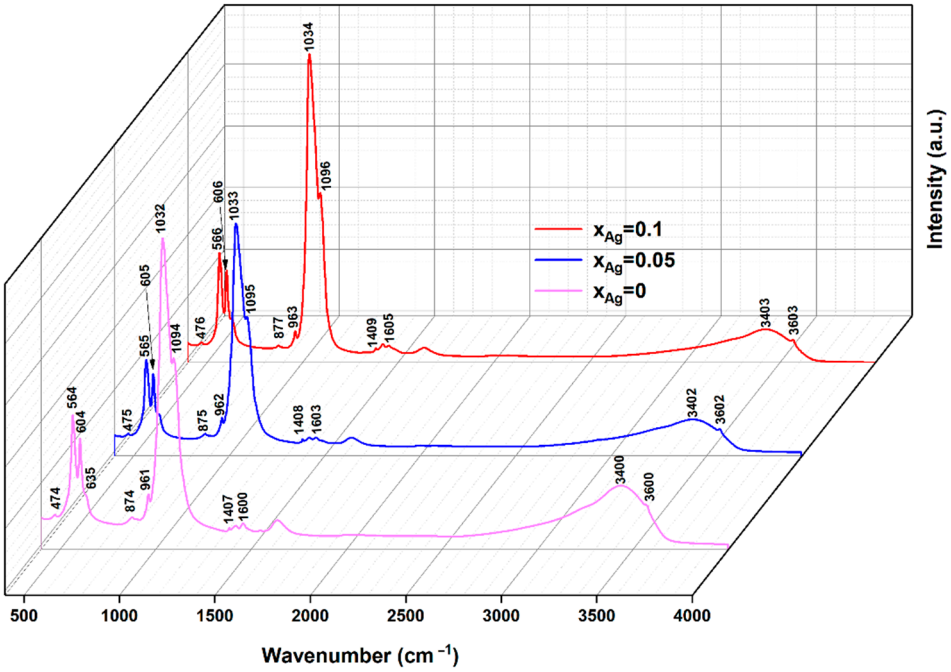

Figure 6. 3D representation of the FTIR spectra of silver doped hydroxyapatite thin films (x_{Ag} = 0; 0.05 and 0.1).

Raman spectroscopy studies added complementary information regarding the molecular structure of the obtained thin films. Therefore, we performed Raman spectroscopy studies on thin layers of silver doped hydroxyapatite. The results are shown in the Figure 7. As mentioned above, we will only discuss the results obtained in the case of pure hydroxyapatite layers, which are similar to those obtained for AgHAp layers. Thus, in Figure 7, the presence of specific maxima of both phosphate and hydroxyl groups from the HAp structure can be noticed.

Therefore, in the obtained Raman spectra the presence of the phosphate group is highlighted by the vibrational bands at around 445 and 432 cm^{-1} that could be attributed to (PO_4^{3-}) ν_2 bending mode. The intense band at around 961 cm^{-1} is characteristic to (PO_4^{3-}) $\nu 1$ bending mode from the hydroxyapatite structure. The peaks at around 615, 591 and 575 cm^{-1} could be attributed to (PO_4^{3-}) ν_4 vibration mode [41,44]. Also, the maxima that are observed at around 1027, 1046, and 1072 cm^{-1} are characteristic to the (PO_4^{3-}) ν_3 stretching mode from the HAp structure [41,44,45]. The sharp vibrational band from 632 cm^{-1} is characteristic to (OH^-) groups present in the HAp samples [41,44]. Thus, the results obtained from both FTIR and Raman spectroscopy studies are in good agreement, both highlighting the purity of the analyzed thin films and the weak influence that dopant (silver) has on the molecular structure of hydroxyapatite.

Implant osseointegration after surgery or infection around the implant are reasons for implantation failure [46]. Thus, it is necessary to develop biocompatible materials to improve osseointegration. In this context, our experimental approach consisted in developing AgHAp thin films on Si substrate to enable biocompatibility with osteoblast cells. We observed that MG63 (ATCC CRL1427) cells grown in the presence of AgHAp thin films do not change their morphology (Figure 8). Also, MG63 (ATCC CRL1427) cells seeded on the covered discs were allowed to grow for 48 h without affecting morphology, even in the case of 0.1 AgHAp sample (Figures 9 and 10). This supports the idea that the

film-coated material is biocompatible, allowing for cell multiplication and tissue recovery with osseointegration of the implant into the surrounding bone. The biocompatibility properties are due to HAp, being well-known as osteoconductive, having the ability to simulate the mineral properties of bones [47,48].

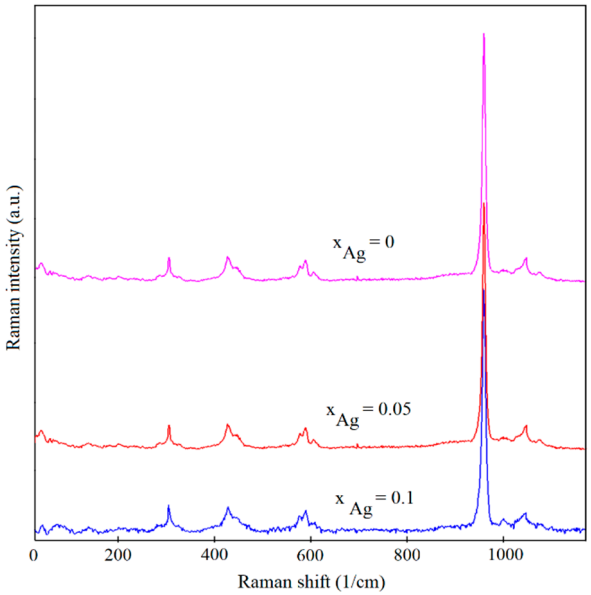

Figure 7. Raman spectra obtained on silver doped hydroxyapatite thin films (x_{Ag} = 0; 0.05 and 0.1).

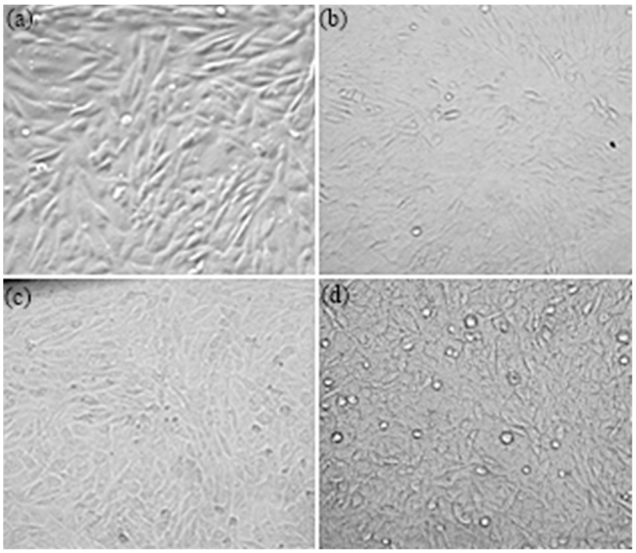

Figure 8. The morphology of MG63 (ATCC CRL1427) cells grown in the presence of the thin films (visible, 200×); control MG63 (ATCC CRL1427) cells (**a**), HAp (**b**), 0.05 AgHAp (**c**), and 0.1 AgHAp (**d**).

As shown in Figure 11, there were no noticeable changes in the percentage of cells in the different cell cycle phases, which supports the results observed by microscopy regarding biocompatibility.

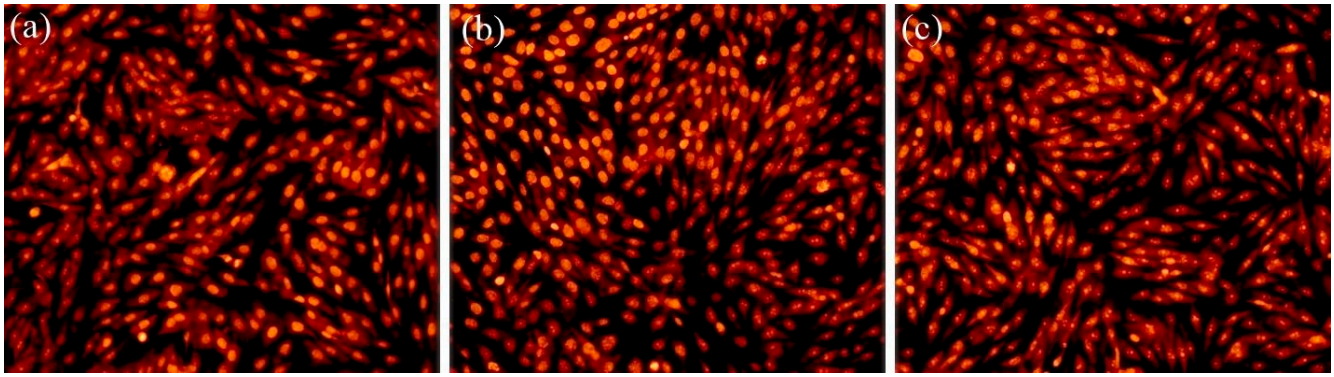

Figure 9. The morphology of MG63 (ATCC CRL1427) cells grown onto HAp (**a**) and 0.05 AgHAp (**b**), and 0.1 AgHAp (**c**) thin films (red filter, PI staining, 200×).

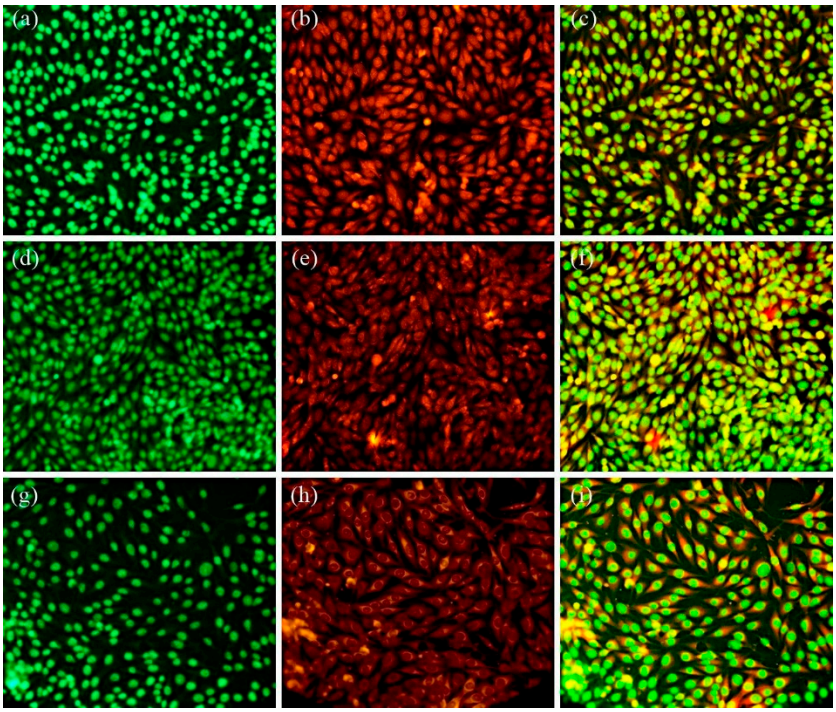

Figure 10. The morphology of MG63 (ATCC CRL1427) cells grown onto HAp (**a**–**c**), 0.05 AgHAp (**d**–**f**), and 0.1 AgHAp (**g**–**i**) (red filter—mitotracker red staining, green filter—acridine orange, 200×).

Additional information about the biocompatibility of the thin films was gathered by AFM studies. For this purpose, the AFM topographies of the thin films' surfaces were acquired at room temperature in normal atmospheric conditions on a surface of 40 μm × 40 μm. The results of the AFM studies are depicted in Figure 12a–f. The 2D AFM images highlighted that on the surface of the investigated thin films, typical patterns of cellular morphology of MG63 (ATCC CRL1427) cells having typical spindle-like shapes were found [49,50]. More than that, the data also suggested that the MG63 (ATCC CRL1427) cells had a good adherence to the samples and proliferated on the surfaces of the HAp, 0.05 AgHAp and 0.1 AgHAp thin films. Furthermore, both the 2D AFM topographies as well as their 3D representations emphasized that the MG63 (ATCC CRL1427) cells were very well spread out and that they formed a monolayer that completely covered the HAp and AgHAp coatings.

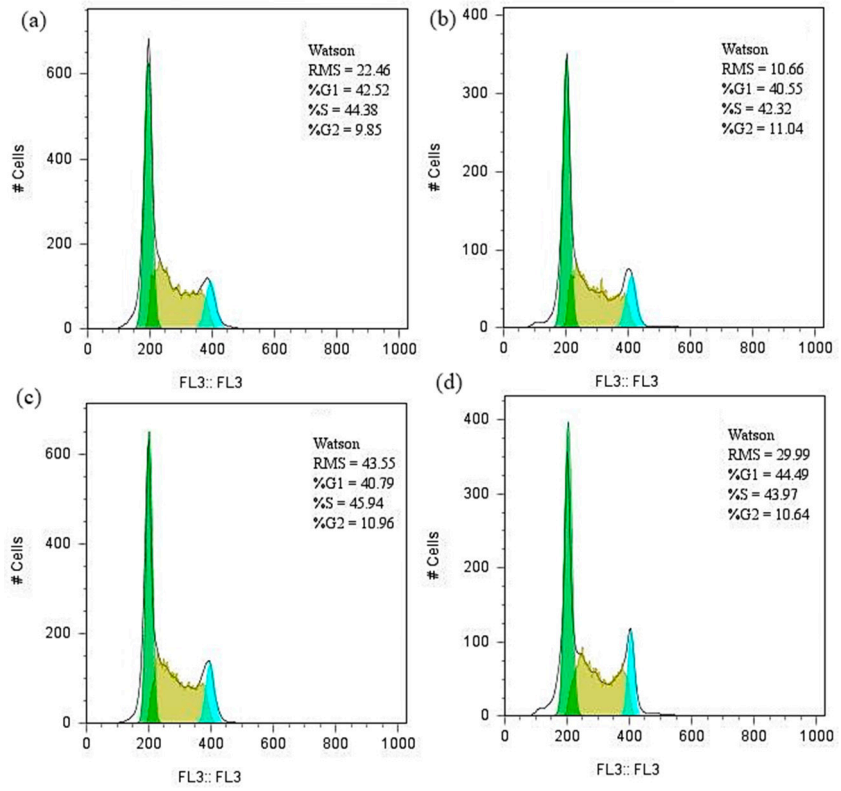

Figure 11. Cell cycle analysis with PI using flow cytometry: uniparametric DNA histograms of propidium iodide intensity (FL3). 0.05 AgHAp (**a**), 0.1 AgHAp (**b**) HAp (**c**), and MG63 (ATCC CRL1427) (**d**).

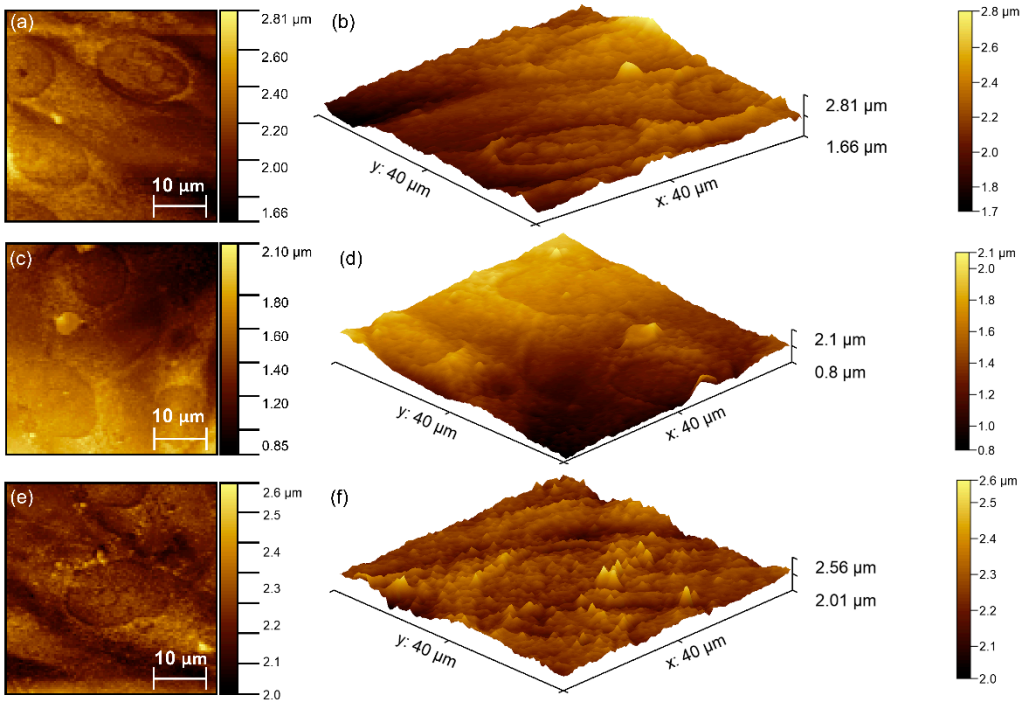

Figure 12. 2D AFM topography of MG63 (ATCC CRL1427) cells grown onto HAp (**a**), 0.05 AgHAp (**c**), 0.1 AgHAp (**e**) coatings and 3D representation of the 2D AFM topographies MG63 (ATCC CRL1427) cells grown onto HAp (**b**), 0.05 AgHAp (**d**), and 0.1 AgHAp (**f**) coatings.

In recent years, a very important factor to be considered in the success of an implant was attributed to the interaction of surrounding tissues and cells with the surface of the

implant and the coatings materials. These issues have raised a lot of attention in both the clinical and experimental settings in the tissue-engineering field. Studies have reported that the surfaces of an implant can directly have a great influence on the surrounding tissue reaction (response), and can considerably affect the quantity and quality of the newly formed tissue. In this context, current treatment plans in implantology involves the use of a biocompatible surface [51] since the surface of the implant plays an important role in the bone response and implant attachment onto the host tissue [52,53].

In a study conducted by Tsukamoto et al. [54], which aims to clarify local and systemic adverse effects of AgHAp coated implants, concentrations of silver in serum and different organs (kidneys, brain, liver and spleen) were evaluated in the acute phase and subacute phase after AgHAp coated titanium rods implantation in rat tibiae. If the silver concentration was increased in serum in the first four days and then decreased, its concentration was increased in the tissues after 28 days of 50% AgHAp coated implants. If silver toxicity depends on the dose, most silver would be gradually excreted. As it can be noticed, the results obtained in our study revealed that silver concentration slightly influences the cell morphology and viability. These results could be attributed to the fact that the presence of silver ions concentration from the samples also influences the morphology of the particles from the thin film, as it was found from XRD results (the average particle size slightly decreased with the increase of silver concentration). More than that, the good biocompatibility of the samples could be attributed both to HAp and to the fact that silver is found in small quantity in the thin films (x_{Ag} = 0.05 and 0.1).

Taking into account on the one hand the results of physico-chemical studies, and on the other hand the results of biological tests, we can conclude that AgHAp thin films could be used as coatings of metal implants (e.g., in stomatology, articulating, hip and shoulder prostheses, etc.). The use of such layers could reduce the risk of post-surgery infection occurrence and could significantly improve the adhesion and proliferation of cells on the implant surface, which would lead to a decrease in orthopedic implant failure. However, future complex studies on AgHAp layers (with various silver concentrations) deposited on surgical titanium (e.g., Ti-6Al-4V alloys) are necessary for a comprehensive understanding of the implant-surrounding tissue interaction.

Nowadays, due to the large spread and constant apparition of multidrug resistant microbial strains, much attention was dedicated to novel antimicrobial materials that could be used in the medical field. In this context, our study also envisaged the antifungal activity of the prepared thin films. For this purpose, one of the most spread fungal strain, *Candida albicans* ATCC 10231 was used for the antifungal assays. The antifungal properties of the HAp, 0.05 AgHAp, and 0.1 AgHAp were assessed after an incubation period of 48 h. The efficiency of the thin films against the *Candida albicans* fungal cells was studied in vitro by both qualitative and quantitative methods. The qualitative evaluation of the *C. albicans* cell's attachment, proliferation and development on the surface of the HAp, 0.05 AgHAp and 0.1 AgHAp thin films was carried out by direct visualization through SEM and CLSM. The results of the SEM studies regarding the adherence and proliferation of the *C. albicans* fungal cells after 48 h of incubation on the surface of HAp, 0.05 AgHAp and 0.1 AgHAp thin films are depicted in Figure 13a–f.

The results of SEM visual observation emphasized that in the case of HAp coatings, the adherence of the fungal cells onto their surface was obviously promoted (in addition to their proliferation). More than that, both the 2D SEM images as well as their 3D representation suggested that the HAp thin films promoted the adherence of the fungal cells and allowed their agglomeration and the formation of fungal biofilm. These results are in good agreement with our previously reported studies regarding the lack of antimicrobial properties of hydroxyapatite [55–57]. The SEM results revealed that both 0.05 AgHAp and 0.1 AgHAp thin films exhibited a strong antifungal activity against *C. albicans* fungal strain. The data showed that after 48 h of incubation, the fungal cells adhered on the surface of 0.05 AgHAp were scarce and isolated and did not show any signs of biofilm formation. More than that, the SEM visualization also highlighted that in the case of

the 0.1 AgHAp thin films, the fungal cells attached on the surface are almost completely eliminated, therefore proving a strong antifungal effect. On the other hand, the results of the SEM visualization also suggested that the antifungal effect of the thin films is correlated with the silver concentration.

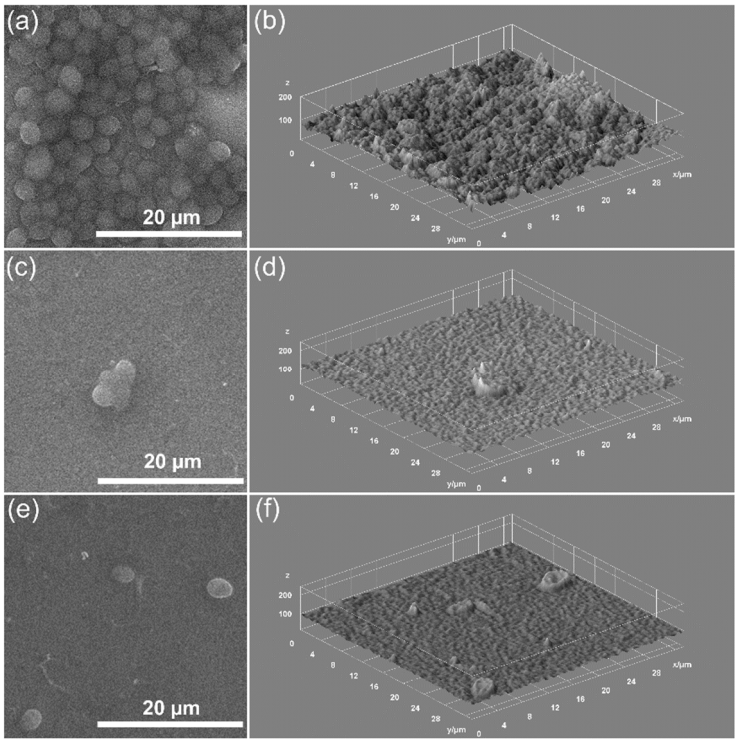

Figure 13. 2D SEM images and 3D representation of SEM images of *Candida albicans* ATCC 10231 cell development on HAp (**a**,**b**), 0.05 AgHAp (**c**,**d**), and 0.1 AgHAp (**e**,**f**) coatings after 48 h of incubation.

Furthermore, complementary information regarding the attachment and development of *C. albicans* fungal cells on the surface of HAp, 0.05 AgHAp, and 0.1 AgHAp thin films were also obtained by CLSM studies. The CLSM investigation clearly showed that the *C. albicans* cells development was strongly inhibited by the presence of both AgHAp thin films and that the 0.05 AgHAp and 0.1 AgHAp thin films did not allow fungal biofilm formation on their surface. The results of the CLSM observation are presented in Figure 14a–f.

On the other hand, CLSM images determined that the HAp thin films promoted and positively influenced the adherence and proliferation on their surface and also that allowed the fungal cells to form biofilm on their surface. These results are in good agreement with the ones obtained by SEM investigation and with our previously reported data [55–57].

Additional information about the antifungal activity of the HAp, 0.05 AgHAp, and 0.1 AgHAp thin films were obtained by performing in vitro quantitative antifungal assays. For this purpose, the thin films were incubated with fungal suspensions and their antifungal properties were assessed by determining the colony forming units (CFU) after 48 h of incubation. The results of the quantitative in vitro antifungal assay are depicted in Figure 15.

The results of the quantitative assays highlighted that the fungal colony forming unit development was inhibited in the case of both 0.05 AgHAp and 0.1 AgHAp thin films. The antifungal assay showed that there was a significant decrease in the number of colonies in the case of both 0.05 AgHAp and 0.1 AgHAp thin films compared to the number of colonies formed in the case of the control culture. Moreover, the data also emphasized that the antifungal activity of 0.1 AgHAp thin films was higher than that of the 0.05 AgHAp thin films after 48 h of incubation with the fungal suspensions. In addition, in good agreement with the qualitative data, the quantitative assays also determined that HAp thin films positively influenced the development of *C. albicans* fungal cells. The data obtained from

the qualitative and quantitative studies demonstrated that the AgHAp thin films strongly inhibited the *C. albicans* fungal strain development, making them an excellent candidate for developing antifungal devices.

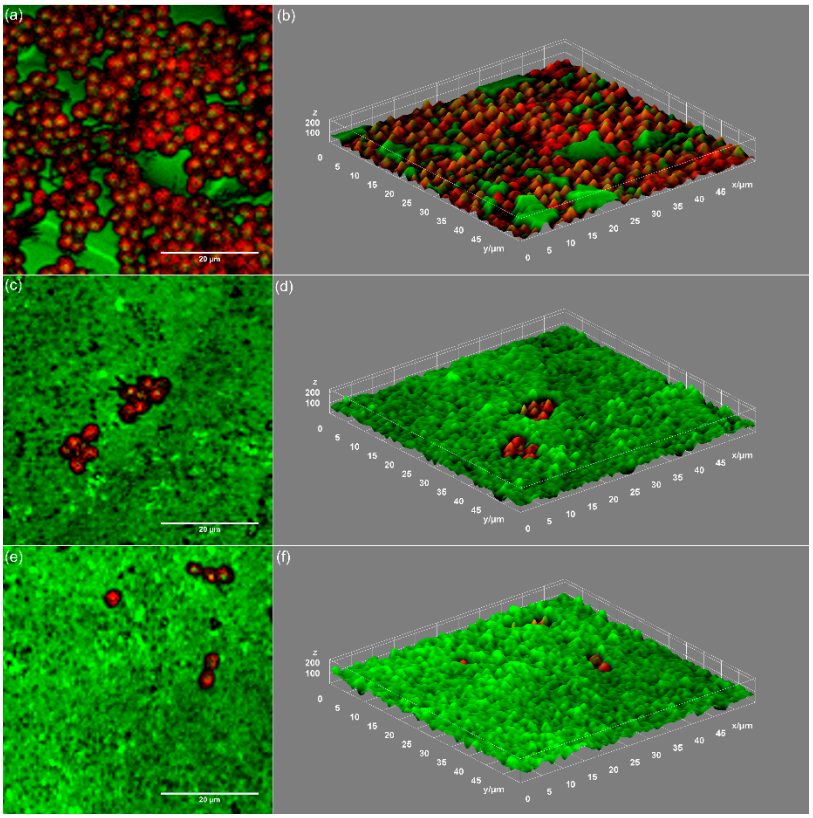

Figure 14. 2D CLSM images and 3D representation of CLSM images of *Candida albicans* ATCC 10231 cell development on HAp (**a**,**b**), 0.05 AgHAp (**c**,**d**), and 0.1 AgHAp (**e**,**f**) coatings after 48 h of incubation.

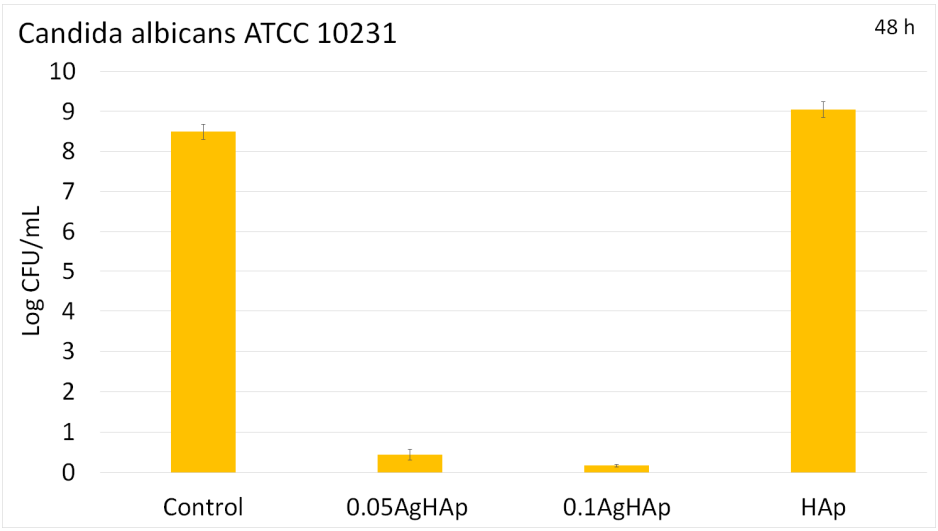

Figure 15. The graphical representation of CFU/mL of HAp, 0.05 AgHAp, and 0.1 AgHAp thin films after 48h of exposure to *Candida albicans* ATCC 10231.

Therefore, the results presented in the current study could contribute to the development of new thin films for innovative biomedical technologies which will positively impact the medical health system worldwide.

4. Conclusions

In this study, we report the obtaining of silver doped hydroxyapatite coatings on Si substrate by a spin coating method. The XRD studies on the obtained coatings showed that particle morphology is ellipsoidal. Moreover, the XPS studies highlighted the presence of silver in 0.05 AgHAp thin films. Furthermore, the analysis of the surface morphology of HAp, 0.05 AgHAp, and 0.1 AgHAp coatings performed by SEM, MM, and AFM emphasized that the obtained coatings are homogenous and continuous with no visible fissures or cracks on their surface. More than that, the SEM data, in agreement with the XRD results, also revealed that the coatings are composed of elongated nanometric particles. The results of both spectroscopic studies performed by FTIR and Raman spectroscopy revealed the presence of the main vibrational molecular bands characteristic to the hydroxyapatite structure (hydroxyl and phosphate groups) in all of the investigated samples. The results of the biological evaluation highlighted that MG63 (ATCC CRL1427) cells were allowed to grow for 48 h on the silver doped hydroxyapatite thin films without affecting the cells morphology. The antifungal effect of HAp and AgHAp thin films against *Candida albicans* ATCC 10231 was also evidenced. Therefore, we can say that AgHAp thin films represent a very promising biocompatible material, which could be successfully used for the development of novel biomedical applications.

Author Contributions: Conceptualization, S.L.I., D.P. and C.B.; methodology, S.L.I., D.P., C.S.C., M.M.-H., R.G. and C.B.; software, S.L.I.; validation, S.L.I., D.P., C.S.C., M.M.-H., R.G. and C.B.; formal analysis, S.L.I., D.P., C.S.C., M.M.-H., R.G. and C.B.; investigation, S.L.I., D.P., C.S.C., M.M.-H., R.G. and C.B.; resources, S.L.I., D.P., C.S.C., M.M.-H., R.G. and C.B.; data curation, S.L.I., D.P., C.S.C., M.M.-H., R.G. and C.B.; writing—original draft preparation, S.L.I., D.P., C.S.C., M.M.-H., R.G. and C.B.; writing—review and editing, S.L.I., D.P., C.S.C. and C.B.; visualization, S.L.I., D.P., C.S.C., M.M-H., R.G. and C.B.; supervision, D.P. and C.B.; project administration, S.L.I., D.P. and C.B.; funding acquisition, D.P. All authors have read and agreed to the published version of the manuscript.

Funding: This work was supported by the Romanian Ministry of Research and Innovation through the project PN-III-P2-2.1-PED-2019-0868 contract number 467PED/2020 and Core Program PN19-030101 (contract 21N/2019).

Institutional Review Board Statement: Not applicable.

Informed Consent Statement: Not applicable.

Data Availability Statement: Not applicable.

Conflicts of Interest: The authors declare no conflict of interest.

References

1. Shi, C.; Gao, J.; Wang, M.; Fu, J.; Wang, D.; Zhu, Y. Ultra-trace silver-doped hydroxyapatite with non-cytotoxicity and effective antibacterial activity. *Mater. Sci. Eng. C* **2015**, *55*, 497–505. [CrossRef]
2. LeGeros, R.Z. Calcium phosphate-based osteoinductive materials. *Chem. Rev.* **2008**, *108*, 4742–4753. [CrossRef] [PubMed]
3. Cao, H.Q.; Zhang, L.; Zheng, H.; Wang, Z. Hydroxyapatite nanocrystals for biomedical applications. *J. Phys. Chem. C* **2010**, *114*, 18352–18357. [CrossRef]
4. Huang, Y.; Qu, Y.; Yang, B.C.; Li, W.; Zhang, B.; Zhang, X.D. In vivo biological responses of plasma sprayed hydroxyapatite coatings with an electric polarized treatment in alkaline solution. *Mater. Sci. Eng. C* **2009**, *29*, 2411–2416. [CrossRef]
5. Simchi, A.; Tamjid, E.; Pishbin, F.; Boccaccini, A.R. Recent progress in inorganic and composite coatings with bactericidal capability for orthopaedic applications. *Nanomedicine* **2011**, *7*, 22–39. [CrossRef] [PubMed]
6. Feng, Q.L.; Cui, F.Z.; Kim, T.N.; Kim, J.W. Ag-substituted hydroxyapatite coatings with both antimicrobial effects and biocompatibility. *J. Mater. Sci. Lett.* **1999**, *18*, 559–561. [CrossRef]
7. Cheng, K.; Weng, W.; Wang, H.; Zhang, S. In vitro behavior of osteoblast-like cells on fluoridated hydroxyapatite coatings. *Biomaterials* **2005**, *26*, 6288–6295. [CrossRef] [PubMed]
8. Kumar, V.B.; Khajuria, D.K.; Karasik, D.; Gedanken, A. Silver and gold doped hydroxyapatite nanocomposites for enhanced bone regeneration. *Biomed. Mater.* **2019**, *14*, 055002. [CrossRef]
9. Min, J.; Choi, K.Y.; Dreaden, E.C.; Padera, R.F.; Braatz, R.D.; Spector, M.; Hammond, P.T. Designer Dual Therapy Nanolayered Implant Coatings Eradicate Biofilms and Accelerate Bone Tissue Repair. *ACS Nano* **2016**, *10*, 4441–4450. [CrossRef] [PubMed]

10. Ribeiro, M.; Ferraz, M.P.; Monteiro, F.J.; Fernandes, M.H.; Beppu, M.M.; Mantione, D.; Sardon, H. Antibacterial silk fibroin/nanohydroxyapatite hydrogels with silver and gold nanoparticles for bone regeneration. *Nanomed. Nanotechnol. Biol. Med.* **2017**, *13*, 231–239. [CrossRef]
11. Geng, H.; Poologasundarampillai, G.; Todd, N.; Devlin-Mullin, A.; Moore, K.L.; Golrokhi, Z.; Gilchrist, J.B.; Jones, E.; Potter, R.J.; Sutcliffe, C.; et al. Biotransformation of silver released from nanoparticle coated titanium implants revealed in regenerating bone. *ACS Appl. Mater. Interfaces* **2017**, *9*, 21169–21180. [CrossRef] [PubMed]
12. Duran, N.; Duran, M.; De Jesus, M.B.; Seabra, A.B.; Favaro, W.J.; Nakazato, G. Silver nanoparticles: A new view on mechanistic aspects on antimicrobial activity. *Nanomed.: Nanotechnol. Biol. Med.* **2016**, *12*, 789–799. [CrossRef] [PubMed]
13. Okada, M.; Matsumoto, T. Synthesis and modification of apatite nanoparticles for use in dental and medical applications. *Jpn. Dent. Sci. Rev.* **2015**, *51*, 85–95. [CrossRef]
14. Kattimani, V.S.; Kondaka, S.; Lingamaneni, K.P. Hydroxyapatite—Past, Present, and Future in Bone Regeneration. *Bone Tissue Regen. Insights* **2016**, *7*, BTRI-S36138. [CrossRef]
15. Gokcekaya, O.; Ueda, K.; Ogasawara, K.; Kanetaka, H.; Narushima, T. In vitro evaluation of Ag-containing calcium phosphates: Effectiveness of Ag-incorporated β-tricalcium phosphate. *Mater. Sci. Eng. C* **2017**, *75*, 926–933. [CrossRef] [PubMed]
16. Ke, D.; Vu, A.A.; Bandyopadhyay, A.; Bose, S. Compositionally graded doped hydroxyapatite coating on titanium using laser and plasma spray deposition for bone implants. *Acta Biomater.* **2019**, *84*, 414–423. [CrossRef]
17. Predoi, D.; Iconaru, S.L.; Predoi, M.V. Fabrication of Silver- and Zinc-Doped Hydroxyapatite Coatings for Enhancing Antimicrobial Effect. *Coatings* **2020**, *10*, 905. [CrossRef]
18. Ciobanu, C.S.; Iconaru, S.L.; Chifiriuc, M.C.; Costescu, A.; Le Coustumer, P.; Predoi, D. Synthesis and antimicrobial activity of silver-doped hydroxyapatite nanoparticles. *BioMed Res. Int.* **2013**, *2013*, 916218. [CrossRef] [PubMed]
19. Rau, J.V.; Cacciotti, I.; Laureti, S.; Fosca, M.; Varvaro, G.; Latini, A. Bioactive, nanostructured Si- substituted hydroxyapatite coatings on titanium prepared by pulsed laser deposition. *J. Biomed. Mater. Res. Part B Appl. Biomater.* **2015**, *103*, 1621–1631. [CrossRef] [PubMed]
20. Zhong, Z.; Qin, J.; Ma, J. Electrophoretic deposition of biomimetic zinc substituted hydroxyapatite coatings with chitosan and carbon nanotubes on titanium. *Ceram. Int.* **2015**, *41*, 8878–8884. [CrossRef]
21. Hoover, S.; Tarafder, S.; Bandyopadhyay, A.; Bose, S. Silver doped resorbable tricalcium phosphate scaffolds for bone graft applications. *Mater. Sci. Eng. C* **2017**, *79*, 763–769. [CrossRef] [PubMed]
22. Chen, Y.; Zheng, X.; Xie, Y.; Ji, H.; Ding, C.; Li, H.; Dai, K. Silver release from silver-containing hydroxyapatite coatings. *Surf. Coat. Technol.* **2010**, *205*, 1892–1896. [CrossRef]
23. Roy, M.; Fielding, G.A.; Beyenal, H.; Bandyopadhyay, A.; Bose, S. Mechanical, in vitro antimicrobial, and biological properties of plasma-sprayed silver-doped hydroxyapatite coating. *ACS Appl. Mater. Interfaces* **2012**, *4*, 1341–1349. [CrossRef]
24. Jamuna-Thevi, K.; Bakar, S.A.; Ibrahim, S.; Shahab, N.; Toff, M.R.M. Quantification of silver ion release, in vitro cytotoxicity and antibacterial properties of nanostuctured Ag doped TiO2 coatings on stainless steel deposited by RF magnetron sputtering. *Vacuum* **2011**, *86*, 235–241. [CrossRef]
25. Hardes, J.; Ahrens, H.; Gebert, C.; Streitbuerger, A.; Buerger, H.; Erren, M.; Gunsel, A.; Wedemeyer, C.; Saxler, G.; Winkelmann, W.; et al. Lack of toxicological side effects in silver-coated mega prostheses in humans. *Biomaterials* **2007**, *28*, 2869–2875. [CrossRef] [PubMed]
26. Qing, T.; Mahmood, M.; Zheng, Y.; Biris, A.S.; Shi, L.; Casciano, D.A. A genomic characterization of the influence of silver nanoparticles on bone differentiation in MC3T3-E1 cells. *J. Appl. Toxicol.* **2018**, *38*, 172–179. [CrossRef] [PubMed]
27. Qin, H.; Zhu, C.; An, Z.; Jiang, Y.; Zhao, Y.; Wang, J.; Liu, X.; Hui, B.; Zhang, X.; Wang, Y. Silver nanoparticles promote osteogenic differentiation of human urine-derived stem cells at noncytotoxic concentrations. *Int. J. Nanomed.* **2014**, *9*, 2469–2478. [CrossRef] [PubMed]
28. Mahmood, M.; Li, Z.; Casciano, D.; Khodakovskaya, M.V.; Chen, T.; Karmakar, A.; Dervishi, E.; Xu, Y.; Mustafa, T.; Watanabe, F.; et al. Nanostructural materials increase mineralization in bone cells and affect gene expression through miRNA regulation. *J. Cell. Mol. Med.* **2011**, *15*, 2297–2306. [CrossRef]
29. Ciobanu, C.S.; Iconaru, S.L.; Massuyeau, F.; Constantin, L.V.; Costescu, A.; Predoi, D. Synthesis, structure and luminescent properties of europium-doped hydroxyapatite nanocrystalline powders. *J. Nanomater.* **2012**, *2012*, 942801. [CrossRef]
30. Iconaru, S.L.; Predoi, M.V.; Motelica-Heino, M.; Predoi, D.; Buton, N.; Megier, C.; Stan, G.E. Dextran-Thyme Magnesium-Doped Hydroxyapatite Composite Antimicrobial Coatings. *Coatings* **2020**, *10*, 57. [CrossRef]
31. Fairley, N.; Fernandez, V.; Richard-Plouet, M.; Guillot-Deudon, C.; Walton, J.; Smith, E.; Flahaut, D.; Greiner, M.; Biesinger, M.; Tougaard, S.; et al. Systematic and collaborative approach to problem solving using X-ray photoelectron spectroscopy. *Appl. Surf. Sci. Adv.* **2021**, *5*, 100112. [CrossRef]
32. ImageJ. Available online: http://imagej.nih.gov/ij (accessed on 10 January 2021).
33. Gwyddion. Available online: http://gwyddion.net/ (accessed on 20 January 2021).
34. Ciobanu, C.S.; Iconaru, S.L.; Predoi, D.; Trușcă, R.-D.; Prodan, A.M.; Groza, A.; Chifiriuc, M.C.; Beuran, M. Fabrication of Novel Chitosan–Hydroxyapatite Nanostructured Thin Films for Biomedical Applications. *Coatings* **2021**, *11*, 1561. [CrossRef]
35. Debye, P.; Scherrer, P. Interference of irregularly oriented particles in X-rays. *Phys. Zeit.* **1916**, *17*, 277–283.
36. Debye, P.; Scherrer, P. Interference on inordinate orientated particles in X-ray light. III. *Phys. Zeit.* **1917**, *18*, 291–301.

37. Danilchenko, S.N.; Kukharenko, O.G.; Moseke, C.; Protsenko, I.Y.; Sukhodub, L.F.; Sulkio-Cleff, B. Determinat ion of the bone mineral crystallite size and lattice strain from diffraction line broadening. *Cryst. Res. Technol.* **2002**, *37*, 1234–1240. [CrossRef]
38. Richardson, J.W.; Faber, J., Jr. *Advances in X-ray Analysis*; Barrett, C.S., Cohen, J.B., Faber, J., Jr., Jenkins, R., Leyden, D.E., Russ, J.C., Predecki, P.K., Eds.; Plenum Publishing: New York, NY, USA, 1986; Volume 29.
39. Ciobanu, C.S.; Massuyeau, F.; Constantin, L.V.; Predoi, D. Structural and physical properties of antibacterial Ag-doped nano-hydroxyapatite synthesized at 100 °C. *Nanoscale Res. Lett.* **2011**, *6*, 613. [CrossRef]
40. Shanmugam, S.; Viswanathan, B.; Varadarajan, T.K. A novel single step chemical route for noble metal nanoparticles embedded organic–inorganic composite films. *Mater. Chem. Phys.* **2006**, *95*, 51–55. [CrossRef]
41. Markovic, M.; Fowler, B.O.; Tung, M.S. Preparation and Comprehensive Characterization of a Calcium Hydroxyapatite Reference Material. *J. Res. Natl. Inst. Stand. Technol.* **2004**, *109*, 553–568. [CrossRef]
42. Bai, X.; More, K.; Rouleau, C.M.; Rabiei, A. Functionally graded hydroxyapatite coatings doped with antibacterial components. *Acta Biomater.* **2010**, *6*, 2264–2273. [CrossRef] [PubMed]
43. Ciobanu, C.S.; Iconaru, S.L.; Pasuk, I.; Vasile, B.S.; Lupu, A.R.; Hermenean, A.; Dinischiotu, A.; Predoi, D. Structural properties of silver doped hydroxyapatite and their biocompatibility. *Mater. Sci. Eng. C* **2013**, *33*, 1395–1402. [CrossRef] [PubMed]
44. Elliot, J. *Structural and Chemistry of Apatites and Other Calcium Ortophosphates*; Elsevier: Amsterdam, The Netherlands, 1994.
45. Ciobanu, C.S.; Iconaru, S.L.; Le Coustumer, P.; Predoi, D. Vibrational Investigations of Silver-Doped Hydroxyapatite with Antibacterial Properties. *J. Spectrosc.* **2013**, *2013*, 471061. [CrossRef]
46. Salaie, R.N.; Besinis, A.; Le, H.; Tredwin, C.; Handy, R.D. The biocompatibility of silver and nanohydroxyapatite coatings on titanium dental implants with human primary osteoblast cells. *Mater. Sci. Eng. C* **2020**, *107*, 110210. [CrossRef] [PubMed]
47. Woodard, J.R.; Hilldore, A.J.; Lan, S.K.; Park, C.; Morgan, A.W.; Eurell, J.A.C.; Clark, S.G.; Wheeler, M.B.; Jamison, R.D.; Johnson, A.J.W. The mechanical properties and osteoconductivity of hydroxyapatite bone scaffolds with multi-scale porosity. *Biomaterials* **2007**, *28*, 45–54. [CrossRef] [PubMed]
48. Hasegawa, M.; Kudo, T.A.; Kanetaka, H.; Miyazaki, T.; Hashimoto, M.; Kawashita, M. Fibronectin adsorption on osteoconductive hydroxyapatite and non-osteoconductive α-alumina. *Biomed. Mater.* **2016**, *11*, 045006. [CrossRef]
49. Surmeneva, M.A.; Kovtun, A.; Peetsch, A.; Goroja, S.N.; Sharonova, A.A.; Pichugin, V.F.; Grubova, I.Y.; Ivanova, A.A.; Teresov, A.D.; Koval, N.N.; et al. Preparation of a silicate-containing hydroxyapatite based coating by magnetron sputtering: Structure and osteoblast-like MG63 cells in vitro study. *RSC Adv.* **2013**, *3*, 11240–11246. [CrossRef]
50. Zhang, L.; Song, Y.; Hosoi, A.; Morita, Y.; Ju, Y. Microwave Atomic Force Microscope: MG63 Osteoblast-like Cells Analysis on Nanometer Scale. *Microsyst. Technol.* **2016**, *22*, 603–608. [CrossRef]
51. Alves, S.F.; Wassall, T. In vitro evaluation of osteoblastic cell adhesion on machined osseointegrated implants. *Braz. Oral Res.* **2009**, *23*, 131–136. [CrossRef] [PubMed]
52. Buser, D.; Schenk, R.K.; Steinemann, S.; Fiorellini, J.P.; Fox, C.H.; Stich, H. Influence of sur-face characteristics on bone integration of tita-nium implants: A histomorphometric study in miniature pigs. *J. Biomed. Mater. Res.* **1991**, *25*, 889–902. [CrossRef]
53. Borsari, V.; Giavaresi, G.; Fini, M.; Torricelli, P.; Salito, A.; Chiesa, R.; Chiusoli, L.; Volpert, A.; Rimondini, L.; Giardino, R. Physical characterization of different-roughness titanium sur-faces, with and without hydroxyapatite coating, and their effect on human osteoblast-like cells. *J. Biomed. Mater. Res. B Appl. Biomater.* **2005**, *75*, 359–368. [CrossRef]
54. Tsukamoto, M.; Miyamoto, H.; Ando, Y.; Noda, I.; Eto, S.; Akiyama, T.; Yonekura, Y.; Sonohata, M.; Mawatari, M. Acute and Subacute Toxicity In Vivo of Thermal-Sprayed Silver Containing Hydroxyapatite Coating in Rat Tibia. *Biomed. Res. Int.* **2014**, *2014*, 902343. [CrossRef]
55. Predoi, D.; Iconaru, S.L.; Predoi, M.V.; Buton, N.; Motelica-Heino, M. Zinc Doped Hydroxyapatite Thin Films Prepared by Sol–Gel Spin Coating Procedure. *Coatings* **2019**, *9*, 156. [CrossRef]
56. Predoi, D.; Iconaru, S.L.; Predoi, M.V.; Groza, A.; Gaiaschi, S.; Rokosz, K.; Raaen, S.; Negrila, C.C.; Prodan, A.-M.; Costescu, A.; et al. Development of Cerium-Doped Hydroxyapatite Coatings with Antimicrobial Properties for Biomedical Applications. *Coatings* **2020**, *10*, 516. [CrossRef]
57. Ciobanu, S.C.; Iconaru, S.L.; Predoi, D.; Prodan, A.M.; Predoi, M.V. Physico-Chemical Properties and In Vitro Antifungal Evaluation of Samarium Doped Hydroxyapatite Coatings. *Coatings* **2020**, *10*, 827. [CrossRef]